CARBON 49 (2011) 147–153

available at www.sciencedirect.com

ScienceDirect

journal homepage: www.elsevier.com/locate/carbon

The chemical vapor infiltration of exfoliated graphite to produce carbon/carbon composites

A.S. Tikhomirov [a,*], N.E. Sorokina [a], O.N. Shornikova [a], V.A. Morozov [a], G. Van Tendeloo [b], V.V. Avdeev [a]

[a] Chemistry Department, Moscow State University, Moscow 119991, Russia
[b] EMAT, University of Antwerp, Groenenborgerlaan 171, B-2020 Antwerp, Belgium

ARTICLE INFO

Article history:
Received 25 March 2010
Accepted 31 August 2010
Available online 7 September 2010

ABSTRACT

Chemical vapor infiltration was used for the production of carbon/carbon composites based on exfoliated graphite and pyrolytic carbon. Two different exfoliated graphites compacted to densities of 0.05–0.4 g/cm^3 were used as a preform. The influence of the synthesis conditions (temperature, pressure, time etc.) on the degree of infiltration, the pyrolytic carbon morphology and the C/C composite characteristics was examined using Raman spectroscopy, scanning electron microscopy and low-temperature nitrogen adsorption.

1. Introduction

Exfoliated graphite (EG), a light foam-like material, found a wide application as a component of sealing materials, catalyst support, oil adsorbent etc. due to its low bulk density of 1–2 g/l, carbon content of 99.9%, developed surface area, peculiar microstructure and an ability to be pressed without a binder into materials with various densities and gas permeability, thermal and electrical conductivity etc. [1–3]. However, a significant disadvantage of EG-based materials limiting their applications is their low strength. Therefore, strengthening with pyrolytic carbon (PC) is a promising way to improve mechanical properties of EG-based composites.

Traditionally EG is produced by exfoliation of graphite intercalation compounds with Brensted acids or expandable graphite. There are two different routs for expandable graphite preparation. The first one consists in a hydrolysis of the intercalation graphite compounds. The second one is an anodic polarization of graphite in the diluted nitric acid solutions [4]. Expandable graphite synthesized according to the second technique possesses imperfect structure and an ability to expand as low as at temperature of 200–250 °C giving EG with highly-developed pore structure and surface area of 90 m^2/g [5].

In order to prepare PC, hydrocarbons, such as natural gas, propane, benzene vapors, chlorine-containing hydrocarbons and their derivatives are subjected to high-temperature decomposition at high pressures followed by condensation on or in a solid support [6–9]. Two distinguished techniques for PC obtaining are known: chemical vapor deposition (CVD) allowing PC surface deposition [10–12] and chemical vapor infiltration (CVI) resulting in infiltration as well as deposition of PC on a support [13–15]. CVD technique is usually carried out in a flow of a carbon source whereas CVI technique requires temperature gradient, potentials or impulse passage of the source.

Recent researches on C/C composites containing PC were mainly focused on composites PC with carbon fibers [16–19], whereas low-dense EG-based materials infiltration is poorly described. Thus, this work is aimed to investigate the general regularities of EG infiltration with PC.

2. Experimental

2.1. Materials

Purified natural graphite with an average flake size of 0.3–0.4 μm and an ash content about 0.29%, nitric acid (d = 1.51

* *Corresponding author:* Fax: +7 495 939 33 16.
E-mail address: tihomir@inbox.ru (A.S. Tikhomirov).
0008-6223/$ - see front matter
doi:10.1016/j.carbon.2010.08.054

or 1.34 g/cm^3), methane were used as parent substances. Two types of EG (EG_N and EG_E) were prepared for EG-based carbon/carbon composites. The nitrate exfoliated graphite (EG_N) with a bulk density of 2.3 g/l was obtained by graphite interaction with 98% nitric acid for 1 h followed by hydrolysis and thermal exfoliation at 1000 °C, according to [20]. The preparation of electrochemical exfoliated graphite (EG_E) with the bulk density of 1.2 g/l was carried out according to the technique described in [4]. The natural graphite was subjected to anodic polarization in 60% HNO_3 up to specific amount of electricity of 500 A·sec/g followed by hydrolysis and exfoliation at 1000 °C.

2.2. C/C composites preparation

EG_N and EG_E were pressed into pellets with densities of 0.05, 0.10, 0.20 and 0.40 g/cm^3. Samples infiltration with PC was carried out according to CVI technique through methane decomposition at temperature of 950–1100 °C and methane pressure of 140–500 mbar. Infiltration time was varied from 15 to 120 min. Saturation of EG samples was performed as a combination of cycles with a duration of 9 s: (1) lap joint (2 s), (2) methane being in a reactor at a constant pressure for t_R = 1–5 s, (3) eviction of unreacted gases and depression creation of 50 mbar (6–2 s). The second period was charged with sample saturation with PC. Methane decomposition was carried out in horizontally situated quartz tube with a length of 1000 mm and diameter of 50 mm.

2.3. Investigation techniques

The specific surface area of EG samples (S_{BET}, m^2/g) before and after PC infiltration was determined by nitrogen adsorption measurements using a Brunauer–Emmett–Teller (BET) equation via QSurf Series analyzer (Thermo Electron Corporation). The samples were preheated in a nitrogen flow at temperature of 250 °C for 3 h. Nitrogen adsorption and desorption were performed at liquid-nitrogen temperature and at room temperature, respectively. Specific surface area was calculated taking into account the samples weight and calibration results. The main characteristics of the different EG samples are presented in Table 1. The bulk density (d_{EG}, kg/m^3) and carbon yield (CY, %) were calculated according to the formulas: $d_{EG} = m_{EG}/V_{EG}$ and $CY = m_{EG}/m_{E\times G}\cdot 100\%$, where m_{EG} is exfoliated graphite mass, V_{EG} is exfoliated graphite volume, $m_{E\times G}$ is expandable graphite mass.

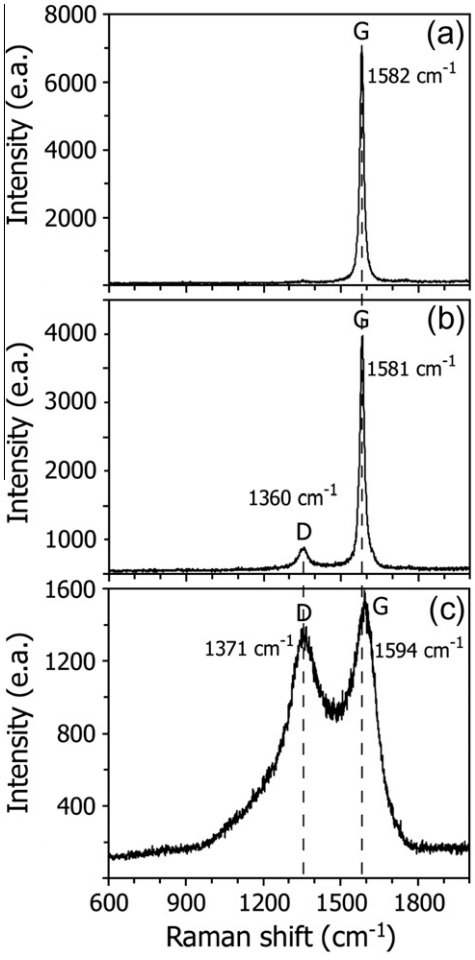

Fig. 1 – Raman-spectra of EG_N (a), EG_E (b) and EG_E–PC composite (c).

Raman-spectra were recorded on a Renishaw InVia microscope using laser with a wavelength of 514 nm (Ar, 20 mWt) with a filter power ND (neutral density) varying from 0.00005 to 100%. Samples investigation was carried out in a backscattering geometry using a confocal microscope Leica DMLM (100′ objective) at an ambient temperature in air. A focal distance was of 250 mm, beam size was varied from 1 to 300 μm. The CCD-camera (576 × 384 px) was used as a detector. The laser radiation power was varied from 0.2 to 30 mWt and spectra accumulation period was of 10–50 s.

Table 1 – Correlation between the bulk density (a), carbon yield (b) and specific surface area (c) of EG pellets of different types.

EG type	d_{EG}[a] (kg/m^3)	CY[b] (wt%)	S_{BET}[c] (m^2/g)	S_{BET} ± 2 (m^2/g)			
				0.05 g/sm^3[d]	0.10 g/sm^3	0.20 g/sm^3	0.40 g/sm^3
EG_N	2.3	86	89	46	36	29	23
EG_E	1.2	61	143	81	54	39	28

[a] Bulk density.
[b] Carbon yield.
[c] Specific surface area.
[d] Density (ρ_0) of EG pellet.

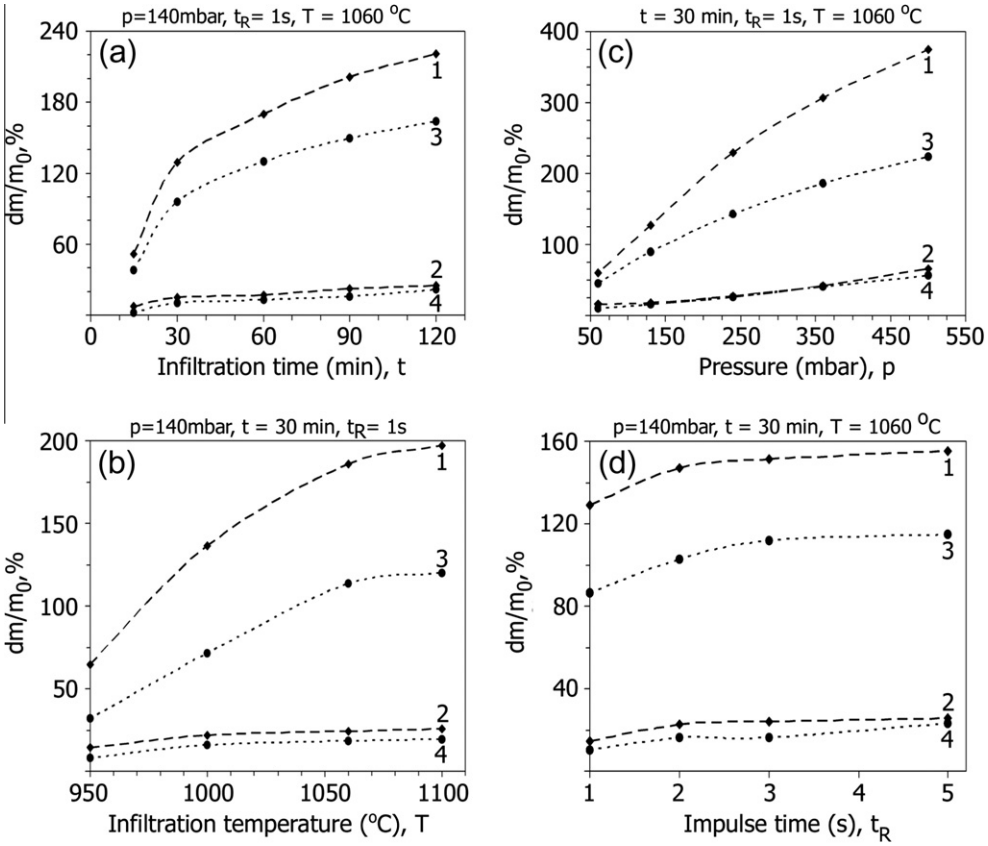

Fig. 2 – The dependences of weigh gain on the infiltration time (a), temperature (b), pressure (c) and impulse time (d) for EG_E (1,2) and EG_N (3,4) pressed to densities of $\rho_0 = 0.05$ g/cm^3 (1,3) and $\rho_0 = 0.2$ g/cm^3 (2,4).

The resonant line position was determined by an experimental spectra description with Gauss and Lorentz functions (pseudo – Voight) using the least-square method in a "WiRE 2.0" soft.

Microstructure of EG–PC composites was observed using a Jeol JEM-5510 scanning electron microscope coupled with an EDX spectrometer (INCA Energy+, energy resolution below 1 eV) at 20 kV accelerated voltage. To observe the microstructure of the EG–PC composites, cross-section samples for SEM observation were prepared by cutting of EG–PC pellets.

3. Results and discussion

3.1. *Exfoliated graphite*

According to the experimental data, EG_N and EG_E are different in bulk densities, specific areas and even in appearances. Specific surface area of EG_E is two times greater than EG_N that is also due to the presence of the amorphous carbon. According to [5] both EG samples are mesoporous and their compacting into pellets leads to the reduction of specific surface area (Table 1). The chemical oxidation of graphite takes place under soft conditions without breaking C/C bonds in the layer whereas EG_E formation flows differently. The anodic polarization of graphite leads not only to the formation of graphite macrocation but also to the formation of functional groups on the graphite surface. The deeper oxidation provides more quantity of surface forms and at the definite conditions the phase of graphite oxide appears. The presence of graphite oxide in the product of graphite anodic polarization gives it extremely low exfoliation temperature of 200–250 °C [4] as a result of exothermal decomposition of graphite oxide. Moreover, this fact also stipulates for the presence of amorphous carbon in EG_E.

Raman spectroscopy reveals differences between EG_N and EG_E (Fig. 1a and b). The peak with a Raman shift of 1581 cm^{-1} (G band) is observed in spectra of both EG samples (Fig. 1a) while the peak with a Raman shift of 1360 cm^{-1} (D band) is found only in the Raman spectrum of EG_E (Fig. 1b). The G peak is the Raman active E_{2g2} mode of graphite involving the in-plane bond-stretching motion of sp^2-hybridized C atoms whilst the D peak is a breathing mode of A_{1g} symmetry involving phonons near the K zone boundary. The appearance of D band in the Raman spectrum of EG_E indicates a high degree of disorder in EG_E or confirms the presence of amorphous carbon with the mixed hybridization [21].

3.2. *EG–PC composites*

3.2.1. *General regularities of EG infiltration with PC*

The dependences of the saturation degree of EG_N and EG_E in terms of the weight gain ($dm/m_0 = (m_{PC}/m_{EG}) \times 100\%$, where m_{PC} and m_{EG} are PC and EG masses, correspondingly) due to PC deposition or infiltration as a functions of the reaction time, temperature, pressure and impulse time are shown in Fig. 2. As one can see, the weight gain significantly increases

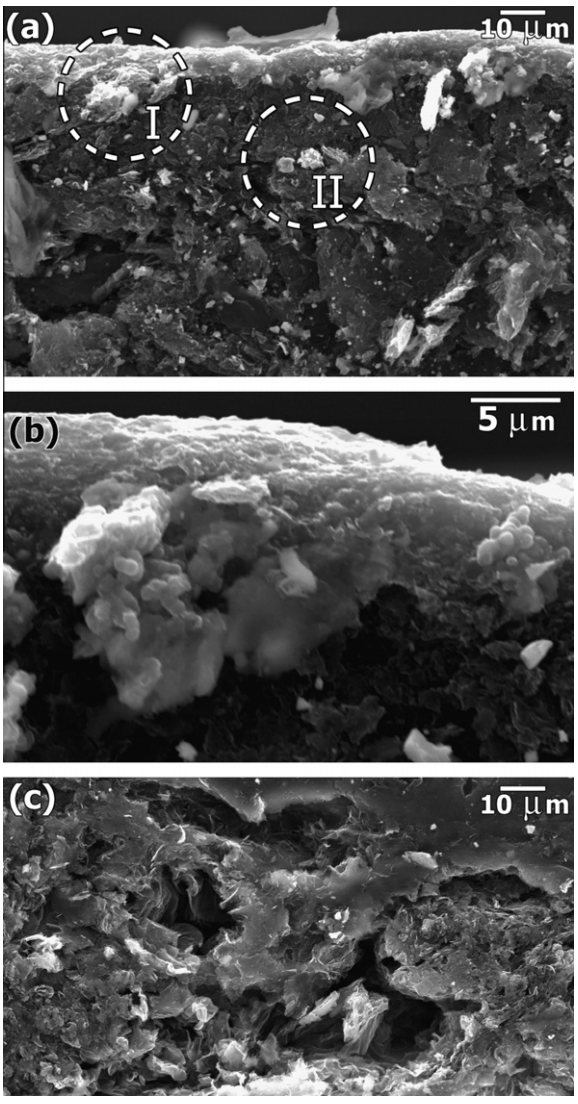

Fig. 3 – SEM cross-section images of sample I: from a sample surface (a); the enlarged image of area I (b); from a sample volume (c).

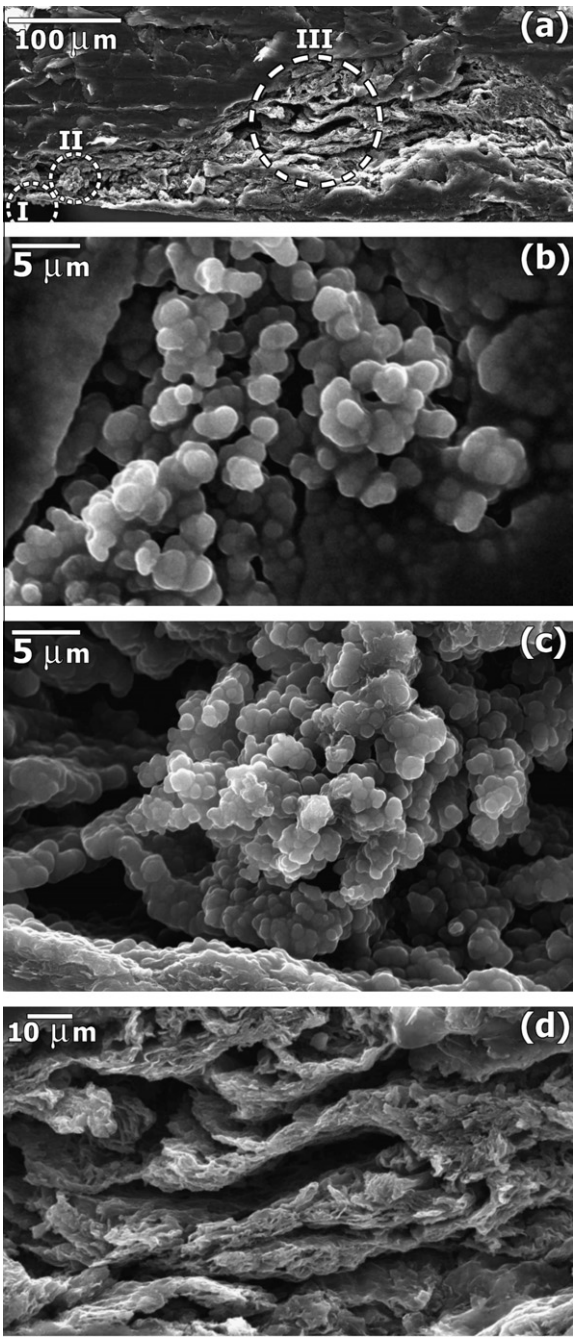

Fig. 4 – SEM images of sample II: a cross-section image from a sample surface (a); the enlarged image from of surface area I (b); the cross-section images of areas II (c) and III (d). Areas I, II, III are marked as dashed cycles in (a).

with the increasing of infiltration time (Fig. 2a), temperature (Fig. 2b) and pressure (Fig. 2c), whereas dm/m_0 does not depend on impulse time (Fig. 2d). Moreover, the weight gain is strictly depends on the methane amount served into reactor and, consequently, amount of products of its decomposition. Using of high pressures, long reaction times and high-temperatures implies a greater CH_4 amount and its complete decomposition. Impulse time primarily has an influence on PC microstructure (Fig. 3–5).

According to Fig. 2 there is a tendency that the saturation of EG_E runs easier than one of EG_N. Nevertheless CVI technique applied for the EG volume infiltration with PC is very sensible to the sample density. The saturation degree of both EG samples with the density of 0.2 g/cm^3 is less than that of samples with the density of 0.05 g/cm^3. Moreover the difference between the saturation degrees of both EG samples with the density of 0.2 g/cm^3 prepared under the similar conditions is insignificant while the weight gains of EG_E are significantly bigger than EG_N. The infiltration of the samples with the density of 0.4 g/cm^3 has shown no difference between EG_E and EG_N. Besides, the weight gains of several percents could be achieved by samples infiltration for at least of 90 min. The increase of the total infiltration time from 15 to 120 min leads to an insignificant weight gain growth although its final value still does not exceed several percents. Hence, the volume infiltration for such pressed samples is practically substituted with a surface deposition. Thus the dependence of the satura-

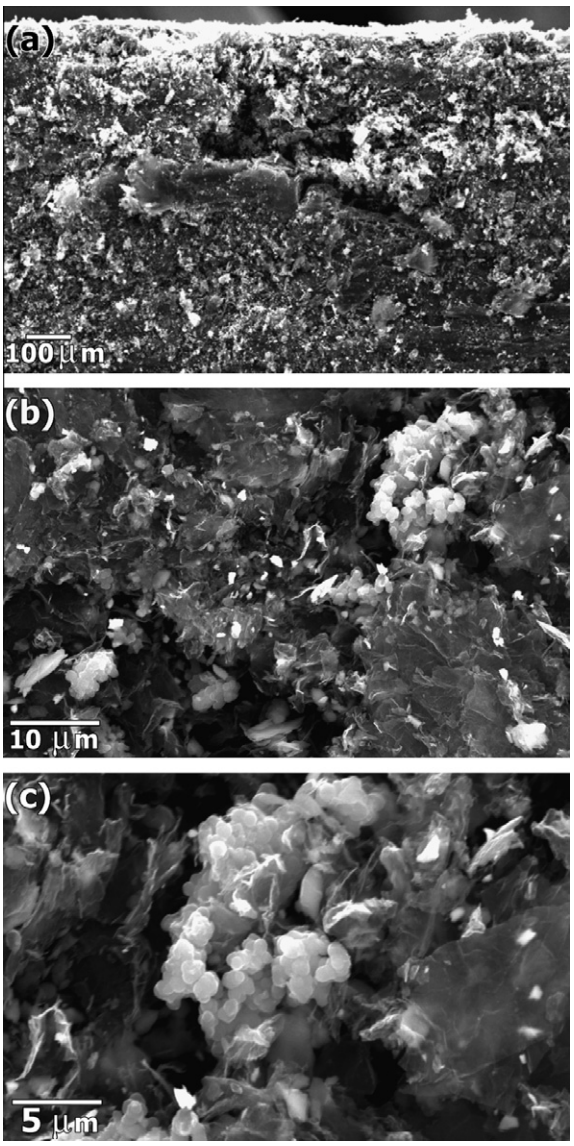

Fig. 5 – SEM cross-section images of sample III with different magnification: 100 (a), 2000 (b) and 4000 (c).

tion degree on EG preparation prehistory disappears with increasing of EG density.

3.2.2. *EG–PC composites structure*

Raman spectroscopy was applied to determine the peculiarity of the carbon atom hybridization in EG–PC composites. Fig. 1c shows a Raman spectrum of the EG–PC composite obtained by EG infiltration with PC at $p = 140$ mbar, $T = 1060$ °C, $t_R = 1$ and reaction time of 30 min. The Raman spectrum of the EG–PC composite significantly differs from the EG_N and EG_E spectra. The G and the D bands in the EG–PC composite spectrum are almost equivalent in intensity. In comparison with EG_E spectrum (Fig. 1b) the D band intensity increases whereas the G band intensity decreases in the Raman spectrum of the EG–PC composite. The increasing of the D band intensity can be explained with the formation of the low-ordered PC amorphous phase. The G and the D bands are shifted and broader leading to a strong overlap. The G band and the D band of the EG–PC composite are located at 1594 cm^{-1} and at 1371 cm^{-1}, respectively, compared with the positions of the EG_E bands at 1581 and 1360 cm^{-1}. According to [22], the G band shift to the area of the greater values of Raman shift is due to the appearance of the sp^3-hybridized C atoms contained in the deposited PC.

3.2.3. *Surface area of the C/C composites*

According to nitrogen adsorption measurements (Table 2), no matter what EG sample was used as a start material, its infiltration with PC leads to the surface area reduction. However, the rate of S_{BET} reduction is higher for the EG_E although the correlation $S_{BET}(EG_E + PC) > S_{BET}(EG_N + PC)$ remains for all the saturation degrees. These are due to the more developed pore structure of the EG_E compared with EG_N. Infiltration of EG with PC apparently occurs with the infill of micro- and mesopores.

3.2.4. *Morphology of the C/C composites*

SEM observations were performed from cross-sections of EG_E + PC composites prepared from EG_E pressed to the density of $\rho_0 = 0.2$ g/cm^3 at infiltration temperature $T = 1060$ °C. SEM cross-section images of EG_E + PC composites prepared under the different conditions (Table 3) are shown in Fig. 3–5. The morphology of the C/C composites is considered using EG_E-based composite due to higher PC content in comparison with EG_N + PC one, although general regularities are similar as it was shown in Fig. 2.

Fig. 3 shows SEM cross-section images of sample I (Table 3). As it is shown in Fig. 3a, under the considered conditions the predominantly surface deposition of PC takes place resulting in the formation of a PC layer with a thickness close to 10 μm (Fig. 3b). The separated PC particles are clearly observed in the area I (Fig. 3a and b). The formation of PC in

Table 2 – Specific surface areas of C/C composites with the density of 0.1 g/cm^3 and various infiltration degrees.

m_{PC}/m_{EG}[a] (%)	ρ_0[b] (g/cm^3)	S_{BET} (EG_N + PC)[c] (m^2/g)	S_{BET} (EG_E + PC)[c] (m^2/g)
0	0.1	35	54
20	0.08	30	45
70	0.06	15	25
240	0.03	–	10

[a] Weight gain.
[b] Density of initial EG pellet.
[c] Specific surface area.

Table 3 – Conditions of the sample preparation for SEM cross-section investigations.

No.	t_R (s)	p (mbar)	t (min)	dm/m_0 (%)	S_{BET} (m^2/g)
I	1	140	90	84.2	19
II	**5**	140	30	77.3	21
III	1	**500**	30	71.6	24

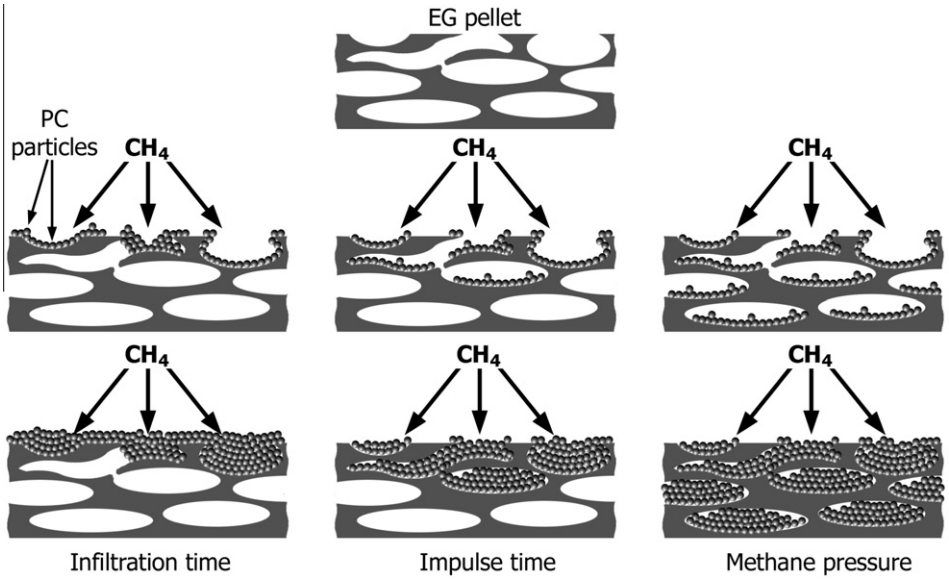

Fig. 6 – Models of the PC particles formation in EG pellets depending on the CVI technique conditions.

sample volume is fragmentary (area II in Fig. 3a) and the macropores infill with PC does not occur (Fig. 3c). Thus the increasing of the infiltration time does not lead to the increasing of methane diffusion depth inside EG_N pellets.

Fig. 4 shows SEM images of sample II (Table 3). According to Fig. 4 the increasing of impulse time provides both surface and volume sample infiltration with PC. The agglomerates of PC spherical particles are observed in the planar and cross-section images (Fig. 4b and c). The maximum infiltration is observed if cracks, apertures or even holes are closed with globes consisting of PC (an outward appearance is "bunch of grapes"). Methane decomposition leads to the infilling by PC the greater part of not only micro- or meso-, but macropores as well. Nevertheless PC agglomerates in sample volume are not observed deeper than at 70–80 μm (Fig. 4a and d). Thus the increasing of impulse time leads to the infilling by PC only near-surface macropores of EG_N pellets.

Fig. 5 shows SEM cross-section images of the EG + PC obtained using the highest pressure applied in the work (sample III in Table 3). Herein the presence of the significant amount of PC not only on the surface but substantially in the volume of the sample should be pointed out. Probably, this is the reason of pore capping in the sample volume. The surface PC layer in contrast to the sample I is not of globular but of lamellar shape. We assume that this peculiarity is due to the well-ordered structure forming during greater impulse duration [7,13,23]. The influence of the different conditions of CVI technique (infiltration time, impulse time and methane pressure) on EG infiltration with PC are summarised in models shown in Fig. 6.

Thus, even long infiltration time does not promote PC penetration into the compacted EG volume. The volume densification of EG could be reached using high pressure in the CVI-process and long impulse time. Under these conditions PC fills or caps pores in EG matrix practically completely, that leads to the PC surface deposition and, as a consequence, decrease of the samples infiltration rate.

4. Conclusions

The influence of temperature, pressure, impulse time and infiltration time on the process of PC deposition on nitrate and electrochemical EG was studied for the first time. EG_E samples are enabled to be infiltrated with PC for shorter time and up to higher infiltration degrees compared to EG_N samples. The maximum difference in infiltration degrees occurs for the low-dense samples ($\rho < 0.2$ g/cm^3) that grades for the samples with high densities. Based on SEM investigations the models of the PC particles formation in EG pellets depending on the CVI technique conditions are proposed. The homogeneous covering of EG support with PC occurs at infiltration durations of 15–30 min, the longer infiltration results in formation of the PC agglomerates filling holes in EG matrix. The mainly volume infiltration occurs under high pressures of 500 mbar; otherwise, PC deposition on support surface takes place. Nitrogen adsorption measurements reveal the significant (2–3 times) reduction of specific area as a result of EG saturation with PC.

Acknowledgements

This work has been performed within the framework of IAP-VI of the Belgian government. Authors are indebted to A.A. Eliseev for the Raman-scattering-investigations.

REFERENCES

[1] Celzard A, Marêché JF, Furdin G. Surface area of compressed expanded graphite. Carbon 2002;40(14):2713–8.
[2] Tryba B, Przepiorski J, Morawski W. Influence of chemically prepared H_2SO_4-graphite intercalation compound (GIC) precursor on parameters of exfoliated graphite (EG) for oil sorption from water. Carbon 2002;41:2013–6.

[3] Afanasov IM, Shornikova ON, Avdeev VV, Lebedev OI, Van Tendeloo G, Matveev AT. Expanded graphite as a support for Ni/carbon composites. Carbon 2009;47(2):513–8.
[4] Sorokina NE, Maksimova NV, Avdeev VV. Anodic oxidation of graphite in 10–98% HNO_3. Inorg Mater 2001;37(4):360–5.
[5] Shornikova ON, Kogan EV, Sorokina NE, Avdeev VV. The specific surface area and porous structure of graphite materials. Russ J Phys Chem 2009;83(6):1022–5.
[6] Lieberman ML, Pierson HO. The chemical vapor deposition of carbon on carbon fibers. Carbon 1975;13(3):159–66.
[7] Oberlin A. Pyrocarbons. Carbon 2002;40:7–24.
[8] Reznik B, Huttinger KJ. On the terminology for pyrolytic carbon. Carbon 2002;40(4):621–4.
[9] Ziegler I, Fournet R, Marquarie P-M. Pyrolysis of propane for CVI of pyrocarbon. Part II. Experimental and modeling study of polyaromatic species. J Anal Appl Pyrolysis 2005;73:231–47.
[10] Bokros JC. Deposition, structure and properties of pyrolytic carbon. Chem Phys Carbon 1969;5:1–118.
[11] Feron O, Langlais F, Naslain R, Thebault J. On kinetic and microstructural transitions in the CVD of pyrocarbon from propane. Carbon 1999;37:1343–53.
[12] Huttinger KJ, Merdes WF. The carbon-steam reaction at elevated pressure: Formations of product gases and hydrogen inhibitions. Carbon 1992;30(6):883–94.
[13] Dupel P, Bourrat X, Pailler P. Structure of pyrocarbon infiltration by pulse-CVI. Carbon 1995;33:1193–204.
[14] Jain-guo Z, Ke-zhi L, He-jun L, Chuang W. The influence of thermal gradient on pyrocarbon deposition in carbon/carbon composites during the CVI process. Carbon 2006;44:786–91.
[15] Brown ARG, Watt W. The preparation and properties of high temperature pyrolytic carbon. London UK: Industrial Carbon and Graphite; 1951:86–100.
[16] Bertrand S, Lavaud JF, Hadi RE, Vignoles G, Pailler R. The thermal gradient-pulse flow CVI process: a new chemical vapor infiltration technique for the densification of fibre preforms. J Eur Ceram Soc 1998;18:857–70.
[17] Ziegler-Devin I, Fournet R, Marquaire P-M. Pyrolysis of propane for CVI of pyrocarbon. Part III: experimental and modeling study of the formation of pyrocarbon. J Anal Appl Pyrolysis 2007;79:268–77.
[18] Bourrat X, Fillion A, Naslain R, Chollon G, Brendlé M. Regenerative laminar pyrocarbon. Carbon 2002;40(15):2931–45.
[19] Zhang WG, Hu ZJ, Huttinger KJ. Chemical vapor infiltration of carbon fiber felt: optimization of densification and carbon microstructure. Carbon 2002;40(14):2529–45.
[20] Sorokina NE, Redchitz AV, Ionov SZ, Avdeev VV. Different exfoliated graphite as a base of sealing materials. J Phys Chem Sol 2006;67:1202–4.
[21] Heimann RB, Evsykov SE, Koga Y. Carbon allotropes: a suggested classification scheme based on valence orbital hybridization. Carbon 1997;35(10–11):1654–8.
[22] Yang DQ, Sacher E. sp-Hybridization in highly oriented pyrolytic graphite and its change on surface modification, as studied by X-ray photoelectron and Raman spectroscopies. Surf Sci 2002;504:125–37.
[23] Delhaes P. Chemical vapor deposition and infiltration processes of carbon materials. Carbon 2002;40:641–57.